OPINION

Towards a mechanistic understanding of the human subcortex

Birte U. Forstmann, Gilles de Hollander, Leendert van Maanen, Anneke Alkemade and Max C. Keuken

Abstract | The human subcortex is a densely populated part of the brain, of which only 7% of the individual structures are depicted in standard MRI atlases. *In vivo* MRI of the subcortex is challenging owing to its anatomical complexity and its deep location in the brain. The technical advances that are needed to reliably uncover this 'terra incognita' call for an interdisciplinary human neuroanatomical approach. We discuss the emerging methods that could be used in such an approach and the incorporation of the data that are generated from these methods into model-based cognitive neuroscience frameworks.

The human subcortex consists of hundreds of unique, small grey matter nuclei[1] that make up approximately 25% of the entire human brain volume[2] (FIG. 1a). Importantly, only approximately 7% of these nuclei are currently represented in standard human brain MRI atlases (for examples, see REF. 3) owing to the technical challenges in imaging these structures. Indeed, the study of basal ganglia networks and nuclei in humans has been frustrated by the fact that these nuclei are difficult to visualize with MRI at field strengths of 3 Tesla (3 T) and below because of their small size and close spatial proximity[4] (FIG. 1b).

The human brain may be mapped at three different levels: the macroscopic, the mesoscopic and the microscopic levels[5]. The macroscopic level is measured in centimetres, which is the scale of large neural networks that spread across the whole brain; the mesoscopic level is measured in millimetres, which is the scale of individual cortical and subcortical nodes; and the microscopic level is measured in micro- and nanometres, which is the scale of individual neurons and neurotransmitters. In this Opinion article, we argue for an approach that combines *in vivo* ultra-high field (UHF) 7 T MRI, post-mortem UHF MRI and post-mortem histology in a model-based cognitive neuroscience framework to capture neurological processes, including decision-making mechanisms, which are implemented in the human subcortex, ranging from the macroscopic to the microscopic level.

One example of mapping these three levels of the human subcortex comes from the study of the regulatory role of basal ganglia networks in spe eded decision making[6–10]. The relatively well-understood cortico–basal ganglia–thalamo–cortical loops are particularly important for decision-making processes, including action selection and inhibition[11,12]. Through the use of the meso- to macroscopic mapping paradigm to assess the role of basal ganglia in action selection, here, we highlight the importance of integrating *in vivo* UHF MRI and post-mortem validation and of placing the resulting data from these approaches into a model-based cognitive neuroscience framework.

We begin by discussing state-of-the-art UHF structural MRI and functional MRI (fMRI) technology and how it can be used to map the human subcortex. We then identify and explain techniques to validate MRI data, including those from post-mortem studies, and end by integrating information from the microscopic, mesoscopic and macroscopic levels into a model-based cognitive neuroscience framework.

Imaging the human subcortex

Neuroimaging and, more broadly, the study of the human subcortex have been particularly challenging for various reasons. Subcortical nuclei are small, they have particular magnetic properties that hinder anatomical identification and functional imaging, and there has been limited availability of reliable automated parcellation procedures, resulting in a large amount of ambiguous data that must be painstakingly and expertly analysed 'by hand'. Moreover, there has been a lack of validation studies, for example, using post-mortem specimens, to confirm MRI findings. This hiatus has many potential causes, including the limited availability of human post-mortem brain specimens and the precariousness of tissue processing, for which the requirements for UHF MRI and histological analyses need to be balanced. Other problems have included a limited knowledge of the function of many subcortical structures, a culture of focusing on cortical structures in MRI-based research (for examples, see REF. 13) and the limited availability of UHF MRI scanners and data. Below, we discuss these issues in more depth and offer some potential solutions to improve the imaging, and understanding, of the subcortex.

MRI data acquisition. The subcortex is a highly dense area with many, very small and distinct nuclei[3], and requires tailored structural MRI contrast images[14]. The use of UHF fMRI combined with UHF structural MRI increases the spatial specificity that can be achieved compared with 3 T approaches[4]. Indeed, previous work directly comparing 3 T fMRI with 7 T fMRI in subcortical areas indicate that, although the latter yields similar activation patterns, it has a higher contrast-to-noise ratio (CNR) and higher spatial specificity[15–17].

Several studies showed that UHF structural MRI improved the visualization of subcortical structures compared with lower field strength MRI[18–24]. Several reasons account for this improvement. The signal-to-noise ratio (SNR) increases linearly with field strength[25]. A high SNR is vitally important as the SNR with structural MRI that can be achieved towards the middle of the brain is substantially lower than the SNR that can be achieved with this technique

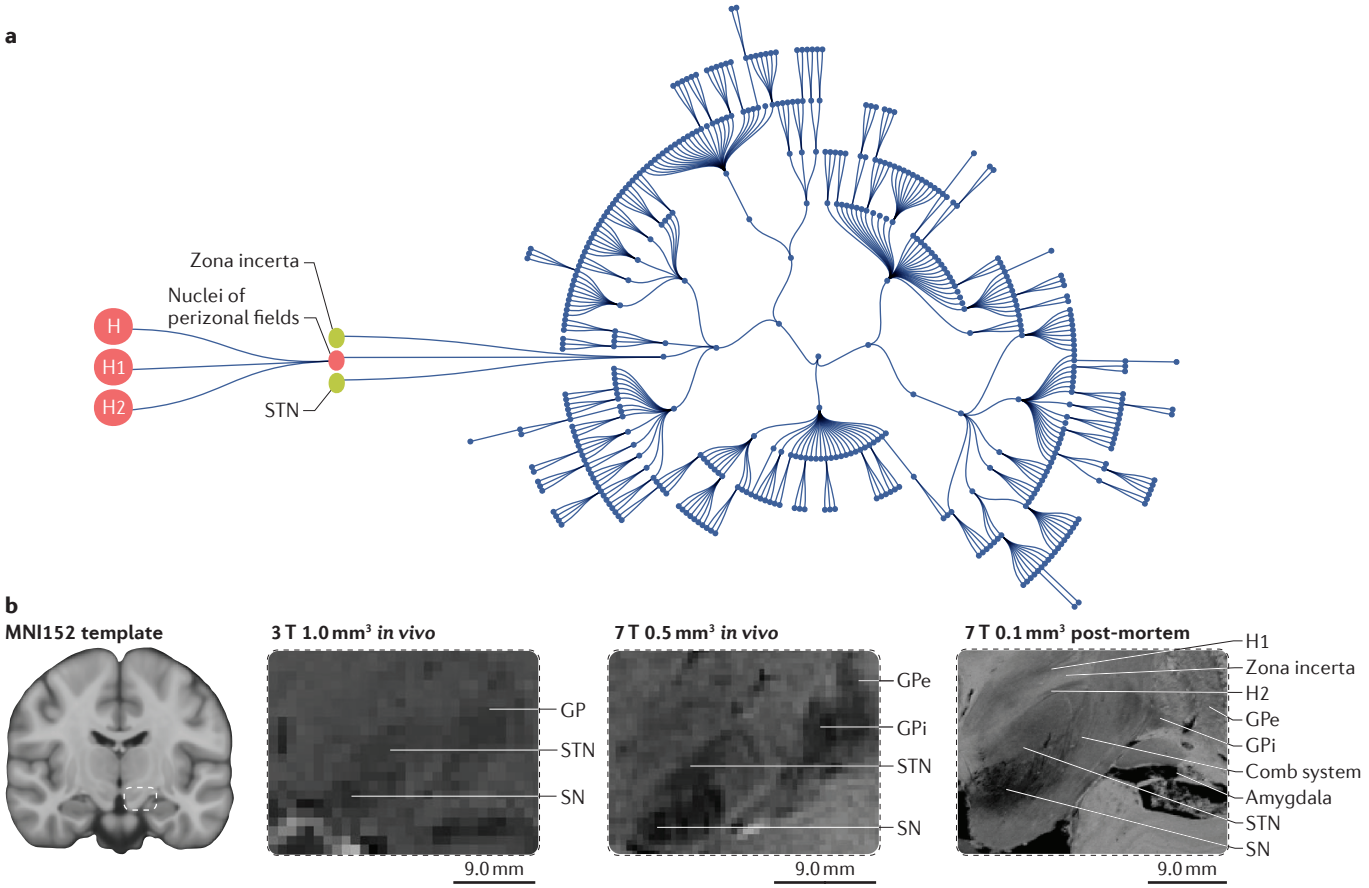

Figure 1 | **Visualization of the human subcortex. a** | A hierarchical tree of the human subcortex is shown. Each node represents 1 of the 445 subcortical structures as defined by the Federative Committee on Anatomical Terminology. The structure of the tree follows the natural anatomical order in which the inner-to-outer direction follows a cascade from larger structures to substructures[1]. For example, the larger nodes on the left represent three small nuclei (in the figure, indicated by 'H', 'H1' and 'H2'), which are the nuclei of the perizonal fields. The nuclei of the perzional fields, together with the zona incerta and the subthalamic nucleus (STN), form the subthalamus. These example nodes were increased in size for visualisation purposes only; no anatomical sizes are implied. **b** | Zoomed-out image presents the MNI152 template. The three coronal zoomed-in scans display the same subcortical region, which is outlined in the dotted line on the MNI152 template. The 3 T *in vivo* 1 mm³ isotropic resolution T2*-weighted structural MRI scan enables the identification of the STN, substantia nigra (SN) and globus pallidus (GP). The 7 T *in vivo* 0.5 mm³ isotropic resolution T2*-weighted structural MRI scan shows increased detail, which now clearly enables the separation of the STN from the SN. The image quality is such that it now also enables the separation of the GP interna (GPi) and GP externa (GPe). Finally, a post-mortem 0.1 mm³ isotropic resolution 7 T T2*-weighted structural MRI scan enables a clear identification of structures that are not visible in either the 3 T or the 7 T *in vivo* scans, such as the zona incerta.

at the cortical level[26]. It is possible to acquire multiple averages on lower field strengths to improve the SNR. However, this is not always practical as the signal-to-thermal noise ratio with 7 T MRI is roughly 2.3 times higher than the value that can be achieved with 3 T MRI. This means that to acquire an image on 3 T MRI with the same contrast (that is, with the same SNR) as a 7 T image, with all else being equal, a 3 T MRI scan needs to be roughly 5.3-fold longer (that is, 2.3^2)[25]. As the scan duration increases, averaging becomes increasingly difficult owing to motion artefacts that are caused by head movements or internal fluid pulsation, which yield image distortions[27,28]. By increasing the SNR, structural imaging with a submillimetre resolution can be achieved, and the delineation of small subcortical structures becomes feasible. Benefiting from the SNR gain and optimized MRI sequences, recent *in vivo* UHF MRI studies on the thalamus have yielded promising results, with the visualisation of several thalamic subnuclei[29–31].

A further advantage of UHF structural MRI can be observed when standard anatomical T1-weighted scans are acquired. The contrast between white and grey matter is sharper in 7 T scans than in 3 T scans owing to the larger difference in T1 relaxation times between the two tissue types in the former[32]. Finally, the increased sensitivity afforded by UHF structural MRI to small field perturbations, which are created by the change in composition between different tissues, means that traditional T1-weighted anatomical scans (which are sensitive to white–grey matter boundaries) can be extended with novel contrast mechanisms such as quantitative susceptibility mapping (QSM)[33,34]. In QSM, the voxel intensity is linearly proportional to the underlying magnetic susceptibility of the tissue, providing a quantitative estimation of iron concentrations[33,35]. As different subcortical nuclei contain different amount of iron and accumulate it at different rates during the adult lifespan[36,37], QSM[38] with high voxel resolution represents an exciting new approach for the visualisation and quantification of the location, shape and morphometric changes of small nuclei (for examples, see REF. 39). Indeed, contrast mechanisms such as QSM enable the visualisation of iron-rich structures such as the basal ganglia, which are otherwise very hard to distinguish on T1-weighted anatomical scans[14,40,41].

UHF diffusion-weighted imaging (DWI) MRI has been conducted in both post-mortem and *in vivo* studies to visualize white matter pathways between different grey matter areas[42–44]. High-resolution DWI enables the visualisation and quantification of highly interconnected structural networks (for examples, see REF. 45) and can be used to inform and constrain the architecture of computational models. DWI can deliver insights into the existence of and the connection strength between cortico–subcortical areas. As with other UHF sequences, UHF DWI MRI benefits from a high SNR[32,46]. This increase in SNR can be used to achieve submillimetre voxel sizes enabling the separation of fine-grained white matter structures such as those in the thalamus[47,48]. Higher field strengths also result in a decrease in the uncertainty of diffusion tensor imaging-estimated parameters, such as fractional anisotropy and principal eigenvectors[46]. In future studies, this information could be included in computational models, enabling concrete predictions of group and individual network dynamics between structures (for a related approach, see REF. 49).

UHF fMRI data acquired along with UHF structural MRI data from the same subjects increases spatial and temporal specificity compared with similar 3 T approaches[4]. Although previous work showed that lower magnetic field strength MRI can yield a spatial resolution that is similar to that achieved by UHF fMRI, the latter approach has several advantages[50,51]. Importantly, 7 T fMRI studies have higher CNR and higher temporal specificity[15–17]. In addition, with equal voxel size, UHF fMRI has superior spatial specificity than lower field strength MRI owing to a smaller point spread function of the blood-oxygen-level-dependent (BOLD) response[52,53]. The BOLD response increases supralinearly with field strength and translates into a higher temporal SNR within a single voxel, increasing the temporal specificity[54,55].

However, the advantages of UHF fMRI are also accompanied by serious challenges[32,56], some of which are particularly relevant for the subcortex[57]. First, owing to the increased sensitivity to susceptibility-induced field differences, there is a greater relative variability of baseline T2* relaxation times across the brain[32,58]. This means that the optimal echo times in fMRI are also more variable across the brain and extremely short in the subcortex; the echo time is approximately 15 milliseconds in the subcortex but approximately 30 milliseconds in the cortex at a field strength of 7 T (REF. 58). Consequently, 7 T fMRI sequences that were originally developed for the cortex are not suitable for fMRI studies of the subcortex. A second, more general challenge of functionally imaging the subcortex is the increased distance to the individual receiving coils and their large overlap in sensitivity profiles compared with the cortex. As a consequence, the signal in small subcortical nuclei is weaker than the signal in cortical areas when using acquisition protocols with higher acceleration factors[59,60]. It is clear that specifically tailored fMRI sequences are necessary when functionally imaging the human subcortex at a UHF.

Combining UHF structural MRI and fMRI has the potential to yield extremely detailed images of the brain: animal studies have already indicated the possibility of single-cell imaging[61], post-mortem human studies have acquired 0.09 mm isotropic voxels[62] and *in vivo* studies have acquired $0.12 \times 0.12 \times 0.6$ mm voxels[63]. The field of UHF MRI is rapidly advancing, and ongoing hardware development together with emerging techniques such as prospective motion correction will ensure continued improvements of the MRI signal[63,64].

MRI data analysis. Automated parcellation procedures aim to enable the automated identification of individual brain structures and provide good results for the cortex but not for the large number of individual subcortical structures[3,40]. Unlike the subcortex, layering principles are constant across the cortex, therefore, automated segmentation tools are simpler to apply[65]. Subcortical structures vary substantially in their histochemical properties, demanding an increase in the number of identity validation studies that are required to determine the anatomical accuracy of parcellation procedures. Given the large number of subcortical structures that exist, manual parcellation becomes an exhaustive and time-consuming process. Automated parcellation procedures would greatly speed up the development of probabilistic atlases of individual subcortical brain structures[40]. Parcellation procedures that are based on statistical shape and appearance models incorporate previously gathered information about the mean and variance of brain region shape and the intensity of such regions on MRI scans[66]. By providing more-detailed information about the anatomical variability such algorithms result in more-accurate parcellation of subcortical structures[40,41,67]. However, to reliably apply these automated procedures further fine-tuning is warranted.

Until now, structural MRI and fMRI data are usually registered into a standard anatomical space. Unfortunately, detailed information about the human subcortex, including changes across the lifespan, is currently missing. Standard MRI atlases, such as the atlas that is used by FreeSurfer software[68], the Harvard–Oxford atlas[69], the LONI Probabilistic Brain Atlas (LPBA40)[70] and the Jülich cytoarchitectonic maps[71], lack detailed information about small subcortical structures. Initial efforts from our group provided manually parcellated probabilistic subcortical maps in both young[14,72] and elderly healthy participants[73]. These efforts have been supplemented with newly developed semiautomated[74] and automated segmentation protocols[40,41] that can be applied to, for example, the striatum, the globus pallidus, the subthalamic nucleus (STN) and the substantia nigra. However, in light of the large intra- and inter-individual variability in the shape, location and tissue composition of these subcortical structures, including the heterogeneous distribution of iron in subcortical nuclei, careful cross-validated manual segmentation protocols will remain vitally important[14,75].

Another general key issue in fMRI analysis is the smoothing of functional data. Historically, smoothing was needed to compensate for the low SNR resulting from low field strength MRI, to meet the assumptions underlying many multiple comparison techniques and to accommodate anatomical variability and registration errors. A recent study showed that smoothing should be avoided in MRI studies, as the signal is blurred to the point where it cannot unequivocally be attributed to specific regions, layers and subcortical nuclei[76–79]. The combination of coarse spatial resolution, smoothing and missing detailed MRI atlases of the subcortex results in a BOLD signal that represents a mix of various neighbouring subcortical nuclei[4]. Even though this is a problem for fMRI at any field strength, it is particularly important to develop techniques that avoid smoothing or improve the accuracy of smoothed functional data as the field of UHF fMRI develops.

Post-mortem validation. Even though *in vivo* UHF MRI can deliver excellent spatial resolution, it does not provide the level of microscopic anatomical detail that is obtained using histological and histochemical approaches. As discussed above, identifying small subcortical nuclei is extremely challenging using *in vivo* UHF MRI scans alone. Therefore, comparing

in vivo results with additional post-mortem UHF MRI images and histochemical data is an important step for the development of increasingly accurate UHF MRI techniques, in which an increasing number of small brain structures become visible. Such validation studies entail the scanning of post-mortem brain tissues using UHF MRI followed by fixation and cutting of the tissue for detailed histological staining. Once scanned and assessed histologically, comparisons between *in vivo* and post-mortem brains can be made. These studies enable confirmation of the identity of individual brain structures based on neurochemical characteristics and organization of neuronal populations. Unfortunately, the field of histology has not developed at the same pace as the field of *in situ* imaging. The crucial importance of 3D information for understanding the structure and function of the brain has not yet led to a major shift in the histological approaches that are used for studying the human brain, and histology is still dominated by 2D techniques. Nevertheless, recent developments are helping to modernize histological research, transforming it from a 2D into a 3D discipline[80,81]. Creating a 3D histological map enables a more direct comparison between histological and MR images, when care is taken to tailor the fixation process.

Tissue-processing procedures require careful optimization to enable post-mortem UHF MRI scanning and subsequent histological processing. Formalin immersion fixation is commonly used for human brain specimens, although this approach may result in uneven fixation, which can be minimized by using small tissue blocks. Both underfixation and overfixation may negatively influence the MRI signal substantially, as well as histological analyses. MRI can be improved by transferring tissues back into a buffered saline solution, and formalin crosslinking can be reversed by heat-induced antigen retrieval to unmask antigens for histochemical purposes[82]. Underfixation results in continued autolysis, cracking and shrinking of the tissues, nuclear chromatin condensation and cellular distortion[83]. Prolonged formalin storage causes coarse hypointensities on T2*-weighted images[84].

Tailoring fixation procedures to the needs of specific MRI protocols, as well as to the needs of histological processing, is possible, particularly as several techniques can be applied to perform antigen retrieval[83]. Highly sensitive immunodetection systems are also available, which allow for lenience towards longer fixation periods[82,85]. Although long fixation times are unfavourable for histochemical processing, they are crucial to prevent MRI artefacts. Factors such as age, sex, ante-mortem disease and cause of death can markedly influence the biochemical properties of the brain[86], and matching for these factors among groups is highly important when comparing biochemical properties (for an example, see REF. 87). However, in the absence of neurodegenerative disease, these factors will not alter the 3D structure of and the connectivity in the brain. In addition, after death, as biochemical properties begin to change rapidly, morphological characteristics are maintained for prolonged periods[88].

Further still, quantitative comparisons can be made. The development of novel contrast measures in quantitative MRI (qMRI)[89] has led to a renewed interest in post-mortem studies, which can be used to validate these techniques. Validation using post-mortem data provides a direct link between tissue characteristics and the measured MRI signal. By providing such links, it becomes possible to quantitatively assess, for example, myelination and iron accumulation directly from *in vivo* UHF structural MRI data. Several studies have been published on the quantification of tissue iron concentrations using various approaches both *in vivo* and post-mortem, and iron concentrations measured in post-mortem tissue samples are consistently found to correlate to susceptibility measures obtained using QSM[33,90]. Exploiting these post-mortem-derived qMRI measures to inform automated segmentation algorithms for *in vivo* data is not trivial, as qMRI parameters can change in accordance with how the tissue is processed[91,92]. In addition, quantifying measures for myelin and neuromelanin have been investigated as markers for neuropathological conditions[91,93,94]. Further studies will have to investigate whether these measures can contribute to our understanding of healthy brain function.

Model-based cognitive neuroscience. Current neuroimaging techniques using UHF 7 T, or higher, MRI can resolve the macroscopic and mesoscopic level with excellent structural and functional detail[95]. At the microscopic level, using post-mortem histology, individual neurons can be distinguished. Fusion of post-mortem and non-invasive UHF MRI techniques can bridge across all three levels of analysis and provide a holistic framework to study the brain by taking into account mechanisms at all relevant scales[80] (FIG. 2).

Formal models can help us to make sense of these large complicated data across all levels. These models allow us to study cognitive processes, including memory encoding, response caution, response inhibition and conflict monitoring, in a formal manner. These models can be fit to behavioural data and enable quantification of the computations and latent variables that underlie cognitive processes. Calculating latent variables using a mathematical model has the key advantage of being able to quantitatively reveal relevant information that cannot be directly measured, such as an individual subject's information processing efficiency during a cognitive task. By relating such individual differences to neural signatures (for example, BOLD activation during a decision-making task), we have learned more about where in the human

Glossary

Blood-oxygen-level-dependent
(BOLD). BOLD imaging refers to MRI contrasts that show changes in the oxygenation of blood, often as a result of neural activity.

Cognitive models
Models that quantify which latent cognitive processes underlie the behaviour in an experimental paradigm.

Contrast-to-noise ratio
(CNR). The difference in signal-to-noise ratio between two areas.

Echo times
The times between magnetic excitation and readout of the signal.

Hypointensities
Lower signal intensities in a specific structure than in the surrounding area.

Parcellation
The process of subdividing the brain in structurally distinct units.

Receiving coils
The magnetic resonance signal in MRI is produced and recorded by two electromagnetic sets of coils: the transmit and the receive coils.

Signal-to-noise ratio
(SNR). The ratio of the strength of the signal of interest to that of the background noise.

T1 relaxation times
The time constant that describes the recovery of the longitudinal component of the net magnetization over time.

T2* relaxation times
The time constant that describes the decay of the transverse component of the net magnetization due to the accumulated phase differences that are caused by spin–spin interactions and local magnetic field inhomogeneities.

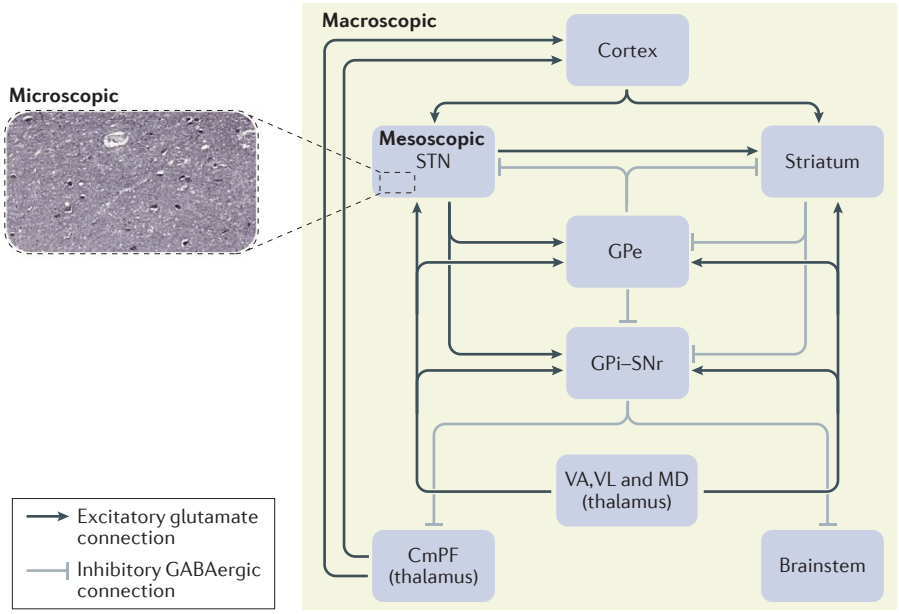

Figure 2 | **A functional theory on cortico–basal ganglia–thalamo–cortical network.** In their default state, the input nuclei of the basal ganglia — that is, the striatum and the subthalamic nucleus (STN) — in combination with the output nuclei of the basal ganglia — that is, the globus pallidus interna (GPi) and the substantia nigra pars reticularis (SNr) — send tonic inhibition to the thalamus, midbrain and brainstem, preventing the premature execution of any action[133]. The black lines indicate excitatory glutamatergic connections, whereas the grey lines indicate inhibitory GABAergic connections. When cortical processes start to favour a certain course of action, this leads to activation of the input nuclei of the basal ganglia (that is, the striatum), which in turn leads to selective suppression of the output nuclei, releasing the brain from inhibition and allowing the action to be executed[134]. The intricate interplay between the different basal ganglia nuclei and the cortical brain areas and layers results in an activation–inhibition network that can generate adaptive changes of response thresholds, thereby allowing swift decision making. The macroscale includes the entire network. The mesoscale focuses on a single nucleus, in this case, the STN. The microscale describes the internal features of a specific nucleus. Detailed knowledge of the microscopic histochemical properties has led to the identification of two types of medium spiny neurons within the substantia nigra, either expressing the dopamine D1 or D2 receptor. The substantia nigra pars compacta is proposed to activate dopamine D1 receptor-expressing cells of the direct pathway and to inhibit the dopamine D2 receptor-expressing neurons of the indirect pathways. The output nuclei GPi and SNr project to the thalamus, which sends efferents completing the cortico–basal ganglia–thalamo–cortical loop. Combining macro-, meso- and micro-scale levels in this way provides a holistic understanding of this network. CmPF, centre median parafascicular nucleus; GPe, globus pallidus externa; MD, mediodorsal nucleus; VA, ventral anterior nucleus; VL, ventral lateral nucleus.

subcortex a task is performed and how cognitive computations and representations are implemented.

Cognitive neuroscience studies the biological substrate underlying cognition[96]. One subfield of cognitive neuroscience that has recently emerged is model-based cognitive neuroscience, which brings together mathematical psychology and cognitive neuroscience, and involves the formalization of cognition through the use of quantitative models[97]. One prominent example of such model is the diffusion decision model (DDM)[98,99]. The DDM simulates how participants make simple, speeded decisions in the following way: subjects accumulate information until a fixed threshold is reached, after which they make a response. Using the DDM, we can now interpret accuracy and response times as two sides of the same coin. When the response threshold is increased, we expect the response times to be longer and the accuracy to increase. Information can also be accumulated at a higher rate, which leads to faster responses and higher accuracy. The DDM can be used to quantitatively estimate these latent cognitive variables, which are called 'response threshold' and 'rate of accumulation'. Such latent cognitive variables capture the elements of decision making that researchers try to understand. This gives us a more nuanced understanding of the cognitive process of speeded decisions than raw behavioural measures such as response time and accuracy can provide. More generally, theoretical and empirical simulation work has also shown that correlations between raw behavioural measures and neural signals can sometimes be deceiving, because they might only index emergent properties of a computational process, as opposed to the computations and their variable representations[100,101]. Other examples of cognitive models deal with learning the value of different choice options[102,103] or cognitive control[104,105].

Another class of models that are used in model-based cognitive neuroscience, the neurocomputational models, provide more focus on how different brain areas interact and could implement cognition, and place little focus on quantitative predictions of behaviour (for examples, see REFS 106,107). One example is the multi-hypothesis sequential probability ratio test (MSPRT) and the mapping of its various components on different nodes in the basal ganglia[9]. The MSPRT explicitly models the excitatory and inhibitory connections between the cortex, the striatum, the globus pallidus, the STN and the substantia nigra, and how this network could calculate the probability of different actions being appropriate for a given task. Although this model can show how behaviour could arise from neural interactions, it is currently not possible to estimate its parameters based on behavioural (or neural) data, like the cognitive models discussed above. The main goal is thus to come up with hypotheses and experiments to validate and/or further test the model predictions.

Both cognitive and neurocomputational models can create a model-based framework in which we can interpret the noisy signals that subcortical fMRI yields, which, when using a model-free approach, may be considered uninterpretable[108]. Recent work in model-based cognitive neuroscience has been successful in linking the role of the basal ganglia to basic cognitive functions as diverse as action selection[99], cognitive control[104] and learning the value of different actions[102,109]. This suggests that a model-based approach is potentially sensitive enough in elucidating the functional role of other subcortical areas, including small nuclei in the brainstem such as the locus coeruleus (for a model-based cognitive neuroscience approach, see REF. 110).

There are three current approaches that exist for making inferences using model-based analyses of fMRI data[108,111]. The first approach is to incorporate neuroanatomical and neurophysiological knowledge in a model. Such models can then yield concrete, testable qualitative predictions by simulation, which can be

investigated experimentally. For example, the now classic neural network simulations that were performed by Frank and colleagues[107] indicate a possible mechanism for how the STN might be involved in inhibiting actions. The plausibility of this mechanism was strengthened by the empirical finding that stimulation of the region in and around the STN, using deep brain stimulation (DBS), alters behaviour in a specific way, exactly as predicted by the simulations[104]. Similar neurocomputational models have been introduced by Bogacz and colleagues[112,113] and by Wang and colleagues (for examples, see REFS 106,114).

The second approach is to regress the parameters of a cognitive model with a neural signal obtained from the subcortex[108,111,115–117]. In contrast to the first approach, the link between the model and the data now no longer hinges only on qualitative predictions about experimental conditions but uses quantitative cognitive models to directly link brain and behavioural data. This second approach provides a mechanistic understanding of cognitive processes that are implemented in brain regions. For example, we have shown that the trial-by-trial fluctuations in activation in the striatum during a moving-dots task can be understood as fluctuations in the amount of 'response caution', a latent decision-making process. This was done by correlating the striatal signal with the trial-by-trial dynamics in the parameters of a mathematical model of decision making[118].

The third and most recent approach in model-based cognitive neuroscience tries to bridge the gap between cognitive models and neurocomputational models by jointly modelling cognitive and neural data[108,111,116,117]. That is, to model behaviour and neural activations as the result of one and the same process. One elegant example is given in a study[119] in which the authors hypothesized that, during a decision-making task, the moment-to-moment evidence for two response options is represented in the firing rate of a specific group of neurons in the frontal eye fields. They found support for this hypothesis by using the actual neural firing rates as the evidence variable in a (slightly modified) DDM. This model was then able to predict trial-to-trial variability in response times and the firing rate of downstream neurons that accumulated the evidence. The authors not only correlated the parameters that were estimated by the model to (summary statistics of) the neural data to suggest some abstract relationship, they went one step further by directly inserting (a transformation of) the neural signal into the cognitive model and equating it to one of its internal variables. The models that are currently developed using this 'joint modelling' approach do not only model neural firing rates and behaviour but also give concrete predictions of the neural firing rates in specific anatomical locations, relating them to specific decision computations[9].

Data availability. 93% of the human subcortex is missing from human MRI atlases and well-validated segmentation algorithms. Filling in the gaps is a time-consuming and costly process. This process would greatly benefit from data sharing[120,121], which would make UHF MRI data sets available for the entire research community and provide possibilities for groups to work on their brain structure of interest without having to acquire high-quality data themselves. In addition, working with existing data allows researchers to conduct power analyses, to simulate MRI parameters to devise new scan sequences tailored to a particular subcortical structure and to perform meta-analyses. Sharing data would thus save both time and funding resources, which could benefit other subcortical research initiatives (TABLE 1).

To facilitate data-sharing efforts, journals entirely dedicated to this purpose have recently been launched, such as *Scientific Data* and *Data in Brief*[120,122–125]. The data 'descriptors' or data papers that are published in these journals are peer-reviewed and aim to provide thorough descriptions of data sets. All these efforts help research groups to compute reproducibility analyses, create subcortical regions of interest for individual studies and (practically) overcome the limited access to UHF MRI scanners (at the time of writing, the number of available UHF MRI scanners worldwide is only approximately 73 but seems to be rapidly increasing, as this number has doubled since 2011 (REF. 126)).

Understanding the human subcortex

An in-depth mechanistic understanding of the human subcortex would provide a wide range of benefits to multiple scientific disciplines. What follows is a brief discussion of just a few of these benefits.

First, small nuclei in the human subcortex, such as the STN, are targets for DBS in patients with Parkinson disease and obsessive–compulsive disorder[127,128]. However, DBS comes at a cost, including some severe adverse effects[129,130]. One possible reason for these effects is the imprecise placement of electrodes in the brain due to the use of preoperative low field structural MRI images for surgical electrode planning. Another possibility is that potential target structures, which are not visible on lower field structural MRI scans, may prove more-effective clinical targets in the future. Testing these hypotheses with a UHF MRI model-based approach would be a step in understanding subcortical mechanisms for the healthy and diseased brain.

Table 1 | **Examples of open-source ultra-high field MRI data sets**

Repository	Example UHF MRI data set	Type of data	Demographics	Refs
Dryad Digital Repository	dx.doi.org/10.5061/dryad.fb41s	T1, T2* and QSM	*n* = 54; age range: 19–75; 24 females	135
International Neuroimaging Data-sharing Initiative (INDI)	dx.doi.org/10.15387/fcp_indi.corr.mpg1	T1 and rsfMRI	*n* = 22; age range: 21–30; 10 females	136
Neuroimaging Informatics Tools and Resources Clearinghouse (NITRC)	nitrc.org/frs/?group_id=606	T1 and T2*	*n* = 28; age range: 21–36; 15 females	137
NeuroVault	neurovault.org/collections/550	Probabilistic atlases for the basal ganglia	*n* = 30; age range: 19–29; 14 females	138
OpenfMRI	openfmri.org/dataset/ds000113/	fMRI and angiography	*n* = 20; age range: 21–38; 8 females	139
Human Connectome	lifespan.humanconnectome.org	rsfMRI and DWI	*n* = 100; age range: 8–75; sex ratio not stated	132

DWI, diffusion-weighted imaging; fMRI functional MRI; QSM, quantitative susceptibility mapping; rsfMRI, resting-state fMRI.

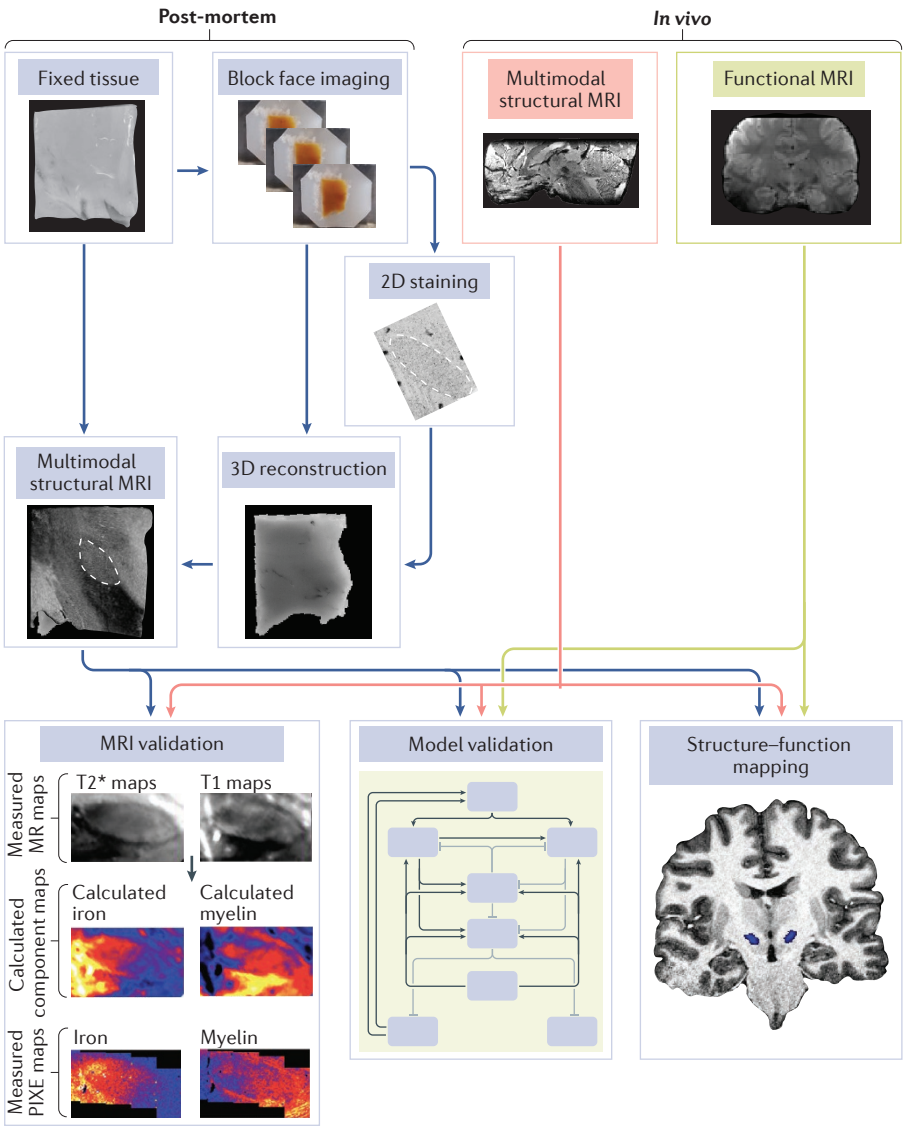

Figure 3 | **Multilevel data acquisition pipeline.** Post-mortem histological stained tissue blocks are combined to create a 3D reconstruction of the fixed tissue, showing the chemical composition and borders of the regions of interest in exact cellular detail. This det ailed picture is compared qualitatively and quantitatively with post-mortem multimodal ultra-high field (UHF) structural MRI scans. *In vivo* multimodal structural MRI data can also be validated by post-mortem data. Histological data not only validate MRI data but also contribute to validating network models (such as those described in FIG. 2), and structural and functional mapping of the brain. Experimental data from *in vivo* UHF functional MRI contribute to validating network models and functional mapping. The combination of post-mortem and *in vivo* data acquisition can provide data on macro-, meso- and microscale levels to create an understanding of an entire network, process and/or brain region of interest in exquisite cellular detail. This approach has the ability to address three questions. First, what is the link between the *in vivo* MRI signal and its underlying anatomical substrate? An example of such a link is whether certain quantitative MRI sequences mainly measure myelin or iron[90]. The subthalamic nucleus is outlined by the dashed line. The second question is: are the biological assumptions that are built in the neurocomputational model valid? An example of such an assumption comes from the computational model of Bogacz and Gurney in which the presence of glutamatergic neurons in the subthalamic nucleus is necessary to predict the activation pattern of the subthalamic nucleus during decision-making tasks[9]. The use of histology can test whether glutamatergic neurons are indeed present, whereas the *in vivo* blood-oxygen-level-dependent (BOLD) measures can be used to test whether the activation patterns match the predictions of the model. The third question is: where is the functional activation located exactly? The use of UHF structural MRI scans that enable the visualization of small structural nuclei will facilitate the creating of more precise atlases. PIXE, particle-induced X-ray emission. The figure in the bottom, left panel (MRI validation) is adapted with permission from REF. 90 (Elsevier).

Second, neuroscientists around the world collaborate to fill our neuroanatomical knowledge gap. One such large-scale collaborative project is the Human Connectome Project[131,132]. The aim of this project is to investigate the connectivity between grey matter areas in a cohort of 1,200 healthy adults using 3 T and 7 T MRI with a multimodal imaging protocol[132]. The Human Connectome Project will undoubtedly provide us with exciting new insights into the functional connections of the human brain. Such a project would evidently benefit from access to well-validated segmentations of all subcortical grey matter structures of the human subcortex. A next step is therefore to develop semiautomated and automated segmentation algorithms that will help to build a UHF MRI subcortex atlas validated with post-mortem data.

Last, knowledge gained from UHF fMRI and structural MRI efforts in health and disease will facilitate the development of explicit neurocomputational models and ultimately lead to new theories of mechanisms of the human subcortex. The MSPRT, the neurocomputational model of decision making proposed by Bogacz and Gurney[9] that was elucidated above, makes specific predictions about excitatory and inhibitory signalling within the cortico–subthalamic–thalamo–cortical network and how they relate to behaviour. An exciting development will be testing concrete model predictions to validate and develop generative cortico–subcortical neurocomputational models for decision making and action selection.

Conclusions

In this Opinion article, we discussed current problems and potential solutions charting the 'terra incognita' that is the human subcortex (FIG. 3). It is evident that a highly interdisciplinary approach — bringing together neuroanatomy, physics, mathematical and experimental psychology, and cognitive and clinical neurosciences — is needed for this challenging endeavour. Such an approach will enable the integration of information over the microscale, mesoscale and macroscale and, as a result, a better mechanistic understanding of the human subcortex.

Birte U. Forstmann, Gilles de Hollander, Anneke Alkemade and Max C. Keuken are at the Amsterdam Brain and Cognition Centre, University of Amsterdam, Nieuwe Achtergracht 129B, 1018 WT Amsterdam, The Netherlands; and at the Netherlands Institute for Neuroscience, an Institute of the Royal Netherlands Academy of Arts and Sciences, Meibergdreef 47, 1105 BA Amsterdam, The Netherlands.

Leendert van Maanen is at the Psychological Methods Department, University of Amsterdam, Nieuwe Achtergracht 129B, 1018 WT Amsterdam, The Netherlands.

Correspondence to B.U.F.
buforstmann@gmail.com

doi:10.1038/nrn.2016.163
Published online 15 Dec 2016

1. Federative Committee on Anatomical Terminology. *Terminologia Anatomica: International Anatomical Terminology* 1st edn (Thieme Stuttgart, 1998).
2. Dunbar, R. I. M. Neocortex size as a constraint on group size in primates. *J. Hum. Evol.* **22**, 469–493 (1992).
3. Alkemade, A., Keuken, M. C. & Forstmann, B. U. A perspective on *terra incognita*: uncovering the neuroanatomy of the human subcortex. *Front. Neuroanat.* http://dx.doi.org/10.3389/fnana.2013.00040 (2013).
4. de Hollander, G., Keuken, M. C. & Forstmann, B. U. The subcortical cocktail problem; mixed signals from the subthalamic nucleus and substantia nigra. *PLoS ONE* **10**, e0120572 (2015).
5. Amunts, K. & Zilles, K. Architectonic mapping of the human brain beyond Brodmann. *Neuron* **88**, 1086–1107 (2015).
6. van Veen, V., Krug, M. K. & Carter, C. S. The neural and computational basis of controlled speed–accuracy tradeoff during task performance. *J. Cogn. Neurosci.* **20**, 1952–1965 (2008).
7. Forstmann, B. U. *et al.* Striatum and pre-SMA facilitate decision-making under time pressure. *Proc. Natl Acad. Sci. USA* **105**, 17538–17542 (2008).
8. Forstmann, B. U. *et al.* Cortico-striatal connections predict control over speed and accuracy in perceptual decision making. *Proc. Natl Acad. Sci. USA* **107**, 15916–15920 (2010).
9. Bogacz, R. & Gurney, K. The basal ganglia and cortex implement optimal decision making between alternative actions. *Neural Comput.* **19**, 442–477 (2007).
10. Bogacz, R., Wagenmakers, E.-J., Forstmann, B. U. & Nieuwenhuis, S. The neural basis of the speed–accuracy tradeoff. *Trends Neurosci.* **33**, 10–16 (2010).
11. Ding, L. & Gold, J. I. The basal ganglia's contributions to perceptual decision making. *Neuron* **79**, 640–649 (2013).
12. Redgrave, P., Prescott, T. J. & Gurney, K. The basal ganglia: a vertebrate solution to the selection problem? *Neuroscience* **89**, 1009–1023 (1999).
13. Johansen-Berg, H. Human connectomics — what will the future demand? *Neuroimage* **80**, 541–544 (2013).
14. Keuken, M. C. *et al.* Quantifying inter-individual anatomical variability in the subcortex using 7 T structural MRI. *Neuroimage* **94**, 40–46 (2014).
15. Baecke, S. *et al.* A proof-of-principle study of multi-site real-time functional imaging at 3 T and 7 T: implementation and validation. *Sci. Rep.* **5**, 8413–8418 (2015).
16. Hahn, A., Kranz, G. S., Seidel, E. M., Sladky, R. & Kraus, C. Comparing neural response to painful electrical stimulation with functional MRI at 3 and 7 T. *Neuroimage* **82**, 336–343 (2013).
17. Hale, J. R. *et al.* Comparison of functional connectivity in default mode and sensorimotor networks at 3 and 7 T. *MAGMA* **23**, 339–349 (2010).
18. Cho, Z. H. *et al.* New brain atlas — mapping the human brain *in vivo* with 7.0 T MRI and comparison with postmortem histology: will these images change modern medicine? *Int. J. Imaging Syst. Technol.* **18**, 2–8 (2008).
19. Cho, Z. H. *et al.* Direct visualization of deep brain stimulation targets in Parkinson disease with the use of 7-tesla magnetic resonance imaging. *J. Neurosurg.* **113**, 639–647 (2010).
20. Kerl, H. U. *et al.* The subthalamic nucleus at 7.0 Tesla: evaluation of sequence and orientation for deep-brain stimulation. *Acta Neurochir.* **154**, 2051–2062 (2012).
21. Kerl, H. U. Imaging for deep brain stimulation: the zona incerta at 7 Tesla. *World J. Radiol.* **5**, 5–16 (2013).
22. Kerl, H. U. *et al.* The subthalamic nucleus at 3.0 Tesla: choice of optimal sequence and orientation for deep brain stimulation using a standard installation protocol. *J. Neurosurg.* **117**, 1155–1165 (2012).
23. Yao, B. *et al.* Susceptibility contrast in high field MRI of human brain as a function of tissue iron content. *Neuroimage* **44**, 1259–1266 (2009).
24. Kerl, H. U., Gerigk, L., Huck, S., Al-Zghloul, M. & Groden, C. Visualisation of the zona incerta for deep brain stimulation at 3.0 Tesla. *Clin. Neuroradiol.* **22**, 55–68 (2012).
25. Edelstein, W. A., Glover, G. H., Hardy, C. J. & Redington, R. W. The intrinsic signal-to-noise ratio in NMR imaging. *Magn. Reson. Med.* **3**, 604–618 (1986).
26. Wiggins, G. C. *et al.* 96-channel receive-only head coil for 3 Tesla: design optimization and evaluation. *Magn. Reson. Med.* **62**, 754–762 (2009).
27. Federau, C. & Gallichan, D. Motion-correction enabled ultra-high resolution *in-vivo* 7 T-MRI of the brain. *PLoS ONE* **11**, e0154974 (2016).
28. Morelli, J. N. *et al.* An image-based approach to understanding the physics of MR artifacts. *Radiographics* **31**, 849–866 (2011).
29. Kanowski, M. *et al.* Direct visualization of anatomic subfields within the superior aspect of the human lateral thalamus by MRI at 7 T. *AJNR Am. J. Neuroradiol.* **35**, 1721–1727 (2014).
30. Tourdias, T., Saranathan, M., Levesque, I. R., Su, J. & Rutt, B. K. Visualization of intra-thalamic nuclei with optimized white-matter-nulled MPRAGE at 7 T. *Neuroimage* **84**, 534–545 (2014).
31. Saranathan, M., Tourdias, T., Bayram, E., Ghanouni, P. & Rutt, B. K. Optimization of white-matter-nulled magnetization prepared rapid gradient echo (MP-RAGE) imaging. *Magn. Reson. Med.* **73**, 1786–1794 (2015).
32. van der Zwaag, W., Schäfer, A., Marques, J. P., Turner, R. & Trampel, R. Recent applications of UHF-MRI in the study of human brain function and structure: a review. *NMR Biomed.* **29**, 1274–1288 (2015).
33. Langkammer, C. *et al.* Quantitative susceptibility mapping (QSM) as a means to measure brain iron? A post mortem validation study. *Neuroimage* **62**, 1593–1599 (2012).
34. Schweser, F., Deistung, A. & Reichenbach, J. R. Foundations of MRI phase imaging and processing for Quantitative Susceptibility Mapping (QSM). *Z. Med. Phys.* **26**, 6–34 (2016).
35. Schweser, F., Deistung, A., Lehr, B. W. & Reichenbach, J. R. Quantitative imaging of intrinsic magnetic tissue properties using MRI signal phase: an approach to *in vivo* brain iron metabolism? *Neuroimage* **54**, 2789–2807 (2011).
36. Zecca, L., Youdim, M., Riederer, P., Connor, J. & Crichton, R. Iron, brain ageing and neurodegenerative disorders. *Nat. Rev. Neurosci.* **5**, 863–873 (2004).
37. Aquino, D. *et al.* Age-related iron deposition in the basal ganglia: quantitative analysis in healthy subjects. *Radiology* **252**, 165–172 (2009).
38. Haacke, E. M. *et al.* Quantitative susceptibility mapping: current status and future directions. *Magn. Reson. Med.* **33**, 1–25 (2015).
39. Hollander, G. *et al.* A gradual increase of iron toward the medial-inferior tip of the subthalamic nucleus. *Hum. Brain. Mapp.* **35**, 4440–4449 (2014).
40. Visser, E. *et al.* Automatic segmentation of the striatum and globus pallidus using MIST: multimodal image segmentation tool. *Neuroimage* **125**, 479–497 (2016).
41. Visser, E., Keuken, M. C., Forstmann, B. U. & Jenkinson, M. Automated segmentation of the substantia nigra, subthalamic nucleus and red nucleus in 7 T data at young and old age. *Neuroimage* **139**, 324–336 (2016).
42. Strotmann, B. *et al.* High-resolution MRI and diffusion-weighted imaging of the human habenula at 7 tesla. *J. Magn. Reson. Imaging* **39**, 1018–1026 (2013).
43. Wargo, C. J. & Gore, J. C. Localized high-resolution DTI of the human midbrain using single-shot EPI, parallel imaging, and outer-volume suppression at 7 T. *Magn. Reson. Imaging* **31**, 810–819 (2013).
44. Dyvorne, H., O'Halloran, R. & Balchandani, P. Ultrahigh field single-refocused diffusion weighted imaging using a matched-phase adiabatic spin echo (MASE). *Magn. Reson. Med.* **75**, 1949–1957 (2015).
45. Keuken, M. C. *et al.* The subthalamic nucleus during decision-making with multiple alternatives. *Hum. Brain. Mapp.* **36**, 4041–4052 (2015).
46. Polders, D. L. *et al.* Signal to noise ratio and uncertainty in diffusion tensor imaging at 1.5, 3.0, and 7.0 Tesla. *J. Magn. Reson. Imaging* **33**, 1456–1463 (2011).
47. Heidemann, R. M., Anwander, A., Feiweier, T., Knösche, T. R. & Turner, R. k-Space and q-space: combining ultra-high spatial and angular resolution in diffusion imaging using ZOOPPA at 7 T. *Neuroimage* **60**, 967–978 (2012).
48. Calamante, F. *et al.* Super-resolution track-density imaging of thalamic substructures: comparison with high-resolution anatomical magnetic resonance imaging at 7.0 T. *Hum. Brain Mapp.* **34**, 2538–2548 (2012).
49. Michalareas, G. *et al.* Alpha-beta and gamma rhythms subserve feedback and feedforward influences among human visual cortical areas. *Neuron* **89**, 384–397 (2016).
50. DeSimone, K., Viviano, J. D. & Schneider, K. A. Population receptive field estimation reveals new retinotopic maps in human subcortex. *J. Neurosci.* **35**, 9836–9847 (2015).
51. De Martino, F. *et al.* Spatial organization of frequency preference and selectivity in the human inferior colliculus. *Nat. Commun.* **4**, 1386–1388 (2015).
52. Engel, S. A., Glover, G. H. & Wandell, B. A. Retinotopic organization in human visual cortex and the spatial precision of functional MRI. *Cereb. Cortex* **7**, 181–192 (1997).
53. Shmuel, A., Yacoub, E., Chaimow, D., Logothetis, N. K. & Ugurbil, K. Spatio-temporal point-spread function of fMRI signal in human gray matter at 7 Tesla. *Neuroimage* **35**, 539–552 (2007).
54. Yacoub, E. *et al.* Imaging brain function in humans at 7 Tesla. *Magn. Reson. Med.* **45**, 588–594 (2001).
55. Uludag, K., Müller-Bierl, B. & Ugurbil, K. An integrative model for neuronal activity-induced signal changes for gradient and spin echo functional imaging. *Neuroimage* **48**, 150–165 (2009).
56. Robitaille, P.-M. & Berliner, L. *Ultra High Field Magnetic Resonance Imaging* (Springer, 2007).
57. Barry, R. L. *et al.* On the origins of signal variance in fMRI of the human midbrain at high field. *PLoS ONE* **8**, e62708 (2013).
58. Peters, A. M. *et al.* T_2* measurements in human brain at 1.5, 3 and 7 T. *Magn. Reson. Imaging* **25**, 748–753 (2007).
59. de Zwart, J. A., van Gelderen, P., Kellman, P. & Duyn, J. H. Application of sensitivity-encoded echo-planar imaging for blood oxygen level-dependent functional brain imaging. *Magn. Reson. Imaging* **48**, 1011–1020 (2002).
60. Pruessmann, K. P., Weiger, M., Scheidegger, M. B. & Boesiger, P. SENSE: sensitivity encoding for fast MRI. *Magn. Reson. Med.* **42**, 952–962 (1999).
61. Shapiro, E. M., Sharer, K., Skrtic, S. & Koretsky, A. P. *In vivo* detection of single cells by MRI. *Magn. Reson. Med.* **55**, 242–249 (2006).
62. Makris, N. *et al.* Volumetric parcellation methodology of the human hypothalamus in neuroimaging: normative data and sex differences. *Neuroimage* **69**, 1–10 (2013).
63. Stucht, D. *et al.* Highest resolution *in vivo* human brain MRI using prospective motion correction. *PLoS ONE* **10**, e0133921 (2015).
64. Frost, R. *et al.* Prospective motion correction and selective reacquisition using volumetric navigators for vessel-encoded arterial spin labeling dynamic angiography. *Magn. Reson. Med.* **76**, 1420–1430 (2015).
65. Cabezas, M., Oliver, A., Lladó, X., Freixenet, J. & Cuadra, M. B. A review of atlas-based segmentation for magnetic resonance brain images. *Comput. Methods Programs Biomed.* **104**, e158–e177 (2011).
66. Heimann, T. & Meinzer, H.-P. Statistical shape models for 3D medical image segmentation: a review. *Med. Image Anal.* **13**, 543–563 (2009).
67. Patenaude, B., Smith, S. M., Kennedy, D. N. & Jenkinson, M. A. Bayesian model of shape and appearance for subcortical brain segmentation. *Neuroimage* **56**, 907–922 (2011).
68. Fischl, B. *et al.* Whole brain segmentation: automated labeling of neuroanatomical structures in the human brain. *Neuron* **33**, 341–355 (2002).
69. Makris, N. *et al.* Decreased volume of left and total anterior insular lobule in schizophrenia. *Schizophr. Res.* **83**, 155–171 (2006).
70. Shattuck, D. W. *et al.* Construction of a 3D probabilistic atlas of human cortical structures. *Neuroimage* **39**, 1064–1080 (2008).
71. Eickhoff, S. B. *et al.* A new SPM toolbox for combining probabilistic cytoarchitectonic maps and functional imaging data. *Neuroimage* **25**, 1325–1335 (2005).

72. Forstmann, B. U. *et al.* Cortico-subthalamic white matter tract strength predict interindividual efficacy in stopping a motor response. *Neuroimage* **60**, 370–375 (2012).
73. Keuken, M. C. *et al.* Ultra-high 7 T MRI of structural age-related changes of the subthalamic nucleus. *J. Neurosci.* **33**, 4896–4900 (2013).
74. Kim, J., Lenglet, C., Duchin, Y., Sapiro, G. & Harel, N. Semiautomatic segmentation of brainsubcortical structures from high-field MRI. *IEEE J. Biomed. Health Inform.* **18**, 1678–1695 (2014).
75. Daugherty, A. M., Haacke, E. M. & Raz, N. Striatal iron content predicts its shrinkage and changes in verbal working memory after two years in healthy adults. *J. Neurosci.* **35**, 6731–6743 (2015).
76. Stelzer, J., Lohmann, G., Mueller, K., Buschmann, T. & Turner, R. Deficient approaches to human neuroimaging. *Front. Hum. Neurosci.* **8**, 462 (2014).
77. Turner, R. in *High-Field MR Imaging* (Springer, 2011).
78. Turner, R. & Geyer, S. Comparing like with like: the power of knowing where you are. *Brain Connect.* **4**, 547–557 (2014).
79. Turner, R. in *Microstructural Parcellation of the Human Cerebral Cortex* (eds Geyer, S. & Turner, R.) (Springer, 2013).
80. Weiss, M. *et al.* Spatial normalization of ultrahigh resolution 7 T magnetic resonance imaging data of the postmortem human subthalamic nucleus: a multistage approach. *Brain Struct. Funct.* **220**, 1695–1703 (2015).
81. Amunts, K. *et al.* BigBrain: an ultrahigh-resolution 3D human brain model. *Science* **340**, 1472–1475 (2013).
82. Shi, S. R., Key, M. E. & Kalra, K. L. Antigen retrieval in formalin-fixed, paraffin-embedded tissues: an enhancement method for immunohistochemical staining based on microwave oven heating of tissue sections. *J. Histochem. Cytochem.* **39**, 741–748 (1991).
83. Chu, W.-S. *et al.* Ultrasound-accelerated formalin fixation of tissue improves morphology, antigen and mRNA preservation. *Mod. Pathol.* **18**, 850–863 (2004).
84. van Duijn, S. *et al.* MRI artifacts in human brain tissue after prolonged formalin storage. *Magn. Reson. Med.* **65**, 1750–1758 (2011).
85. Hauptmann, G., Lauter, G. & Söll, I. Detection and signal amplification in zebrafish RNA FISH. *Methods* **98**, 50–59 (2016).
86. Ravid, R., Van Zwieten, E. J. & Swaab, D. F. Brain banking and the human hypothalamus — factors to match for, pitfalls and potentials. *Prog. Brain Res.* **93**, 83–95 (1992).
87. Alkemade, A. *et al.* AgRP and NPY expression in the human hypothalamic infundibular nucleus correlate with body mass index, whereas changes in αMSH are related to type 2 diabetes. *J. Clin. Endocrinol. Metab.* **97**, E925–E933 (2012).
88. Kretzschmar, H. Brain banking: opportunities, challenges and meaning for the future. *Nat. Rev. Neurosci.* **10**, 70–78 (2009).
89. Weiskopf, N., Mohammadi, S., Lutti, A. & Callaghan, M. F. Advances in MRI-based computational neuroanatomy. *Curr. Opin. Neurol.* **28**, 313–322 (2015).
90. Stüber, C. *et al.* Myelin and iron concentration in the human brain: a quantitative study of MRI contrast. *Neuroimage* **93**, 95–106 (2014).
91. Schmierer, K. *et al.* Quantitative magnetic resonance of postmortem multiple sclerosis brain before and after fixation. *Magn. Reson. Med.* **59**, 268–277 (2008).
92. Dawe, R. J., Bennett, D. A., Schneider, J. A., Vasireddi, S. K. & Arfanakis, K. Postmortem MRI of human brain hemispheres: T_2 relaxation times during formaldehyde fixation. *Magn. Reson. Med.* **61**, 810–818 (2009).
93. Keren, N. I. *et al.* Histologic validation of locus coeruleus MRI contrast in post-mortem tissue. *Neuroimage* **113**, 235–245 (2015).
94. Mottershead, J. P. *et al.* High field MRI correlates of myelin content and axonal density in multiple sclerosis. *J. Neurol.* **250**, 1293–1301 (2003).
95. Plantinga, B. R. *et al.* Ultra-high field magnetic resonance imaging of the basal ganglia and related structures. *Front. Hum. Neurosci.* **8**, 1–22 (2014).
96. Gazzaniga, M., Ivry, R. & Mangun, G. *Cognitive Neuroscience* (MIT Press, 2007).
97. Forstmann, B. U. & Wagenmakers, E.-J. (eds) *An Introduction to Model-Based Cognitive Neuroscience* (Springer, 2015).
98. Ratcliff, R. A theory of memory retrieval. *Psychol. Rev.* **85**, 59–108 (1978).
99. Forstmann, B. U., Ratcliff, R. & Wagenmakers, E.-J. Sequential sampling models in cognitive neuroscience: advantages, applications, and extensions. *Annu. Rev. Psychol.* **67**, 641–666 (2016).
100. Marr, D. *Vision: a Computational Investigation into the Human Representation and Processing of Visual Information* (San Francisco, 1982).
101. Jonas, E. & Kording, K. Automatic discovery of cell types and microcircuitry from neural connectomics. *eLife* **4**, e04250 (2015).
102. O'Doherty, J. *et al.* Dissociable roles of ventral and dorsal striatum in instrumental conditioning. *Science* **304**, 452–454 (2004).
103. Sutton, R. S. & Barto, A. G. *Introduction to Reinforcement Learning* (MIT Press, 1998).
104. Cavanagh, J. F. *et al.* Subthalamic nucleus stimulation reverses mediofrontal influence over decision threshold. *Nat. Neurosci.* **14**, 1462–1467 (2011).
105. Logan, G. D. & Cowan, W. B. On the ability to inhibit thought and action: a theory of an act of control. *Psychol. Rev.* **91**, 295–327 (1984).
106. Lo, C. C. & Wang, X. J. Cortico–basal ganglia circuit mechanism for a decision threshold in reaction time tasks. *Nat. Neurosci.* **9**, 956–963 (2006).
107. Frank, M. J. Hold your horses: a dynamic computational role for the subthalamic nucleus in decision making. *Neural Netw.* **19**, 1120–1136 (2006).
108. de Hollander, G., Forstmann, B. U. & Brown, S. D. Different ways of linking behavioral and neural data via computational cognitive models. *Biol. Psychiatry Cogn. Neurosci. Neuroimaging* **1**, 101–109 (2016).
109. Frank, M. J. *et al.* fMRI and EEG predictors of dynamic decision parameters during human reinforcement learning. *J. Neurosci.* **35**, 485–494 (2015).
110. Mittner, M., Hawkins, G. E., Boekel, W. & Forstmann, B. U. A. A neural model of mind wandering. *Trends Cogn. Sci.* **20**, 570–578 (2016).
111. Turner, B. M., Forstmann, B. U., Love, B. C., Palmeri, T. J. & Van Maanen, L. Approaches to analysis in model-based cognitive neuroscience. *J. Math. Psychol.* http://dx.doi.org/10.1016/j.jmp.2016.01.001 (2016).
112. Bogacz, R., Usher, M., Zhang, J. & McClelland, J. Extending a biologically inspired model of choice: multi-alternatives, nonlinearity and value-based multidimensional choice. *Phil. Trans R. Soc. B* **362**, 1655–1670 (2007).
113. Bogacz, R., Hu, P., Holmes, P. & Cohen, J. Do humans produce the speed–accuracy trade-off that maximizes reward rate? *Q. J. Exp. Psychol.* **63**, 863–891 (2010).
114. Wei, W., Rubin, J. E. & Wang, X. J. Role of the Indirect pathway of the basal ganglia in perceptual decision making. *J. Neurosci.* **35**, 4052–4064 (2015).
115. Turner, B. M., Rodriguez, C. A., Norcia, T. M., McClure, S. M. & Steyvers, M. Why more is better: simultaneous modeling of EEG, fMRI, and behavioral data. *Neuroimage* **128**, 96–115 (2016).
116. Turner, B. M. *et al.* A Bayesian framework for simultaneously modeling neural and behavioral data. *Neuroimage* **72**, 193–206 (2013).
117. Turner, B. M., van Maanen, L. & Forstmann, B. U. Informing cognitive abstractions through neuroimaging: the neural drift diffusion model. *Psychol. Rev.* **122**, 312–336 (2015).
118. van Maanen, L. *et al.* Neural correlates of trial-to-trial fluctuations in response caution. *J. Neurosci.* **31**, 17488–17495 (2011).
119. Purcell, B. A. *et al.* Neurally constrained modeling of perceptual decision making. *Psychol. Rev.* **117**, 1113–1143 (2010).
120. Candela, L., Castelli, D., Manghi, P. & Tani, A. Data journals: a survey. *J. Assoc. Inf. Sci. Technol.* **66**, 1747–1762 (2015).
121. Poldrack, R. A. & Gorgolewski, K. J. Making big data open: data sharing in neuroimaging. *Nat. Neurosci.* **17**, 1510–1517 (2014).
122. Poline, J.-B. *et al.* Data sharing in neuroimaging research. *Front. Neuroinform.* **6**, 9 (2012).
123. Eickhoff, S., Nichols, T. E., Van Horn, J. D. & Turner, J. A. Sharing the wealth: neuroimaging data repositories. *Neuroimage* **124**, 1065–1068 (2016).
124. [No authors listed.] More bang for your byte. *Sci. Data* **1**, 140010 (2014).
125. Wang, H.-R. "Publish or perish": should this still be true for your data? *Data Brief* **1**, 85–86 (2014).
126. Duyn, J. H. The future of ultra-high field MRI and fMRI for study of the human brain. *Neuroimage* **62**, 1241–1248 (2012).
127. Bronstein, J. M. *et al.* Deep brain stimulation for Parkinson disease: an expert consensus and review of key issues. *Arch. Neurol.* **68**, 165 (2011).
128. de Koning, P. P., Figee, M., van den Munckhof, P., Schuurman, P. R. & Denys, D. Current status of deep brain stimulation for obsessive–compulsive disorder: a clinical review of different targets. *Curr. Psychiatry Rep.* **13**, 274–282 (2011).
129. Groiss, S. J., Wojtecki, L., Südmeyer, M. & Schnitzler, A. Deep brain stimulation in Parkinson's disease. *Ther. Adv. Neurol. Disord.* **2**, 20–28 (2009).
130. Christen, M., Bittlinger, M., Walter, H., Brugger, P. & Müller, S. Dealing with side effects of deep brain stimulation: lessons learned from stimulating the STN. *AJOB Neurosci.* **3**, 37–43 (2012).
131. Sporns, O., Tononi, G. & Kötter, R. The human connectome: a structural description of the human brain. *PLoS Comput. Biol.* **1**, e42 (2005).
132. Van Essen, D. C. *et al.* The Human Connectome Project: a data acquisition perspective. *Neuroimage* **62**, 2222–2231 (2012).
133. Chevrier, A. D., Noseworthy, M. D. & Schachar, R. Dissociation of response inhibition and performance monitoring in the stop signal task using event-related fMRI. *Hum. Brain Mapp.* **28**, 1347–1358 (2007).
134. Mink, J. W. The basal ganglia: focused selection and inhibition of competing motor programs. *Prog. Neurobiol.* **50**, 381–425 (1996).
135. Forstmann, B. U. *et al.* Multi-modal ultra-high resolution structural 7-Tesla MRI data repository. *Sci. Data* **1**, 140050–140058 (2014).
136. Gorgolewski, K. J. *et al.* A high resolution 7-Tesla resting-state fMRI test-retest dataset with cognitive and physiological measures. *Sci. Data* **2**, 140054 (2015).
137. Tardif, C. L. *et al.* Open Science CBS Neuroimaging Repository: sharing ultra-high-field MR images of the brain. *Neuroimage* **124**, 1143–1148 (2016).
138. Keuken, M. C. & Forstmann, B. U. A probabilistic atlas of the basal ganglia using 7 T MRI. *Data Brief* **4**, 577–582 (2015).
139. Hanke, M. *et al.* A high-resolution 7-Tesla fMRI dataset from complex natural stimulation with an audio movie. *Sci. Data* **1**, 140003 (2014).

Acknowledgements

The authors thank A. Schäfer, R. Trampel and W. van der Zwaag for helpful discussion about this manuscript and R. Mulray who assisted in proofreading of the manuscript. The authors' research was supported by an ERC grant from the European Research Council (B.U.F.), a Vidi grant from the Dutch Organization for Scientific Research (B.U.F.), a grant by the dutch Hersenstichting (B.U.F. and A.A.), and the Dutch Parkinson Funds (B.U.F. and A.A.).

Competing interests statement

The authors declare no competing interests.

FURTHER INFORMATION

Federative International Programme on Anatomical Terminology: http://fipat.library.dal.ca/about/
Human Connectome Project: http://humanconnectomeproject.org

ALL LINKS ARE ACTIVE IN THE ONLINE PDF